https://doi.org/10.5194/acp-2022-275
Preprint. Discussion started: 26 April 2022

Atmospheric Chemistry and Physics Discussions

Radiative impact of improved global parameterisations of oceanic dry deposition of ozone and lightning-generated NO_x

Ashok K. Luhar[1], Ian E. Galbally[1], Matthew T. Woodhouse[1]

[1]CSIRO Oceans and Atmosphere, Aspendale, 3195, Australia

Correspondence to: Ashok K. Luhar (ashok.luhar@csiro.au)

Abstract. We investigate the impact of recent process-based and empirical improvements to oceanic ozone dry deposition parameterisation and lightning-generated NO_x (LNO_x) parameterisation on radiative fluxes by conducting a 5-year simulation of the global ACCESS-UKCA chemistry-climate model with radiative feedbacks of ozone and methane included. Both parameterisations increase the global net downward top-of-the-atmosphere (TOA) radiative flux, akin to instantaneous radiative forcing, compared to the base parameterisations. The dry deposition improvement results in a relatively small increase of 4.3 mW m^{-2} in the net downward TOA radiative flux. But this increases to 86 mW m^{-2} when the improved LNO_x parameterisation (which increases the LNO_x production from 4.8 to 6.9 Tg N yr^{-1}) is also used. For comparison, this estimated difference in the radiative flux is equivalent to ~18% of the anthropogenic effective radiative forcing (ERF) due to ozone over the years 1750–2019 reported by the Intergovernmental Panel on Climate Change (IPCC) Sixth Assessment Report (AR6). Other global changes from the use of the two parameterisations include an increase in the downward longwave radiation and a decrease in the downward shortwave radiation at the Earth's surface, and a decrease of 0.64 years in the methane lifetime against loss due to the hydroxyl radical, with changes being larger in magnitude in the tropics. Although the total global LNO_x production may be the same, how LNO_x is distributed spatially makes a difference to radiative transfer. The changes in radiation components and methane lifetime per unit change in LNO_x and column ozone are also calculated. We estimate that the uncertainty range in the net downward TOA radiation due to reported uncertainty range in global estimates of LNO_x could be as much as 238 mW m^{-2}. LNO_x has a significant influence on the atmospheric lifetime of CH_4, and the value of LNO_x used within a model will influence the ERF and global warming potential of anthropogenic methane.

https://doi.org/10.5194/acp-2022-275
Preprint. Discussion started: 26 April 2022

Atmospheric Chemistry and Physics Discussions

1 Introduction

Apart from water vapour, carbon dioxide (CO_2), methane (CH_4), ozone (O_3), nitrous oxide (N_2O), and fluorinated gases are the principal greenhouse gases in the atmosphere. Being radiatively active, these gases play an important role in the Earth's energy budget and hence climate system. Together with aerosols, their concentrations govern the impedance to transfer and loss from the atmosphere of radiative energy. A radiative forcing broadly refers to a change in the top-of-the-atmosphere (TOA) energy budget as a result of an imposed anthropogenic or natural perturbation, for example, changes in aerosol or greenhouse gas concentrations, in downwelling solar radiation, or in land use). The climate system responds to this change by cooling or warming. In the Sixth Assessment Report (AR6) of the United Nations Intergovernmental Panel on Climate Change (IPCC), an effective radiative forcing (ERF) is termed as a change in net downward radiative flux at the TOA following a perturbation, including effects of any adjustments in both tropospheric and stratospheric temperatures, water vapour, clouds, and some surface properties, for example surface albedo from vegetation changes, but excluding any changes due to the global surface air temperature change (Forster et al., 2021). According to AR6, the total abundance-based anthropogenic ERF due to increases in long-lived well-mixed greenhouse gases over the years 1750–2019 is 3.32 ± 0.29 W m^{-2}, of which 2.16 ± 0.26 W m^{-2} is due to CO_2, 0.54 ± 0.11 W m^{-2} to CH_4, 0.21 ± 0.03 W m^{-2} to N_2O and 0.41 ± 0.08 W m^{-2} to total halogens (Forster et al., 2021). Ozone is a short-lived climate forcer (SLCF) (chemical lifetime of about 22 days in the troposphere), and its anthropogenic ERF for the same period is estimated to be 0.47 ± 0.23 W m^{-2}, almost all (95%) of which is due to tropospheric O_3 changes. Thus, tropospheric O_3 provides the third largest anthropogenic ERF, and overall O_3 represents about 16% of the net anthropogenic ERF of 2.72 ± 0.76 W m^{-2}, the latter includes an aerosol ERF of -1.1 ± 0.6 W m^{-2} (Forster et al., 2021).

Ozone interacts with down-welling and up-welling solar (or shortwave) and terrestrial (or longwave) radiation. Any changes in the atmospheric distribution of O_3 contribute to changes in its radiative impact. Compared to the long-lived and well-mixed greenhouse gases, O_3 exhibits a highly spatially inhomogeneous distribution in the troposphere because of its short chemical lifetime compared to transport timescales, and therefore, it has strong radiative effects on regional scales.

Ozone is not emitted directly into the atmosphere but is formed in both the stratosphere and troposphere by photochemical reactions involving natural and anthropogenic precursor species. Ozone is an oxidant as well as a precursor to the formation of hydroxyl and hydroperoxyl radicals which play a critical role in the tropospheric chemical cycles of many trace gases, e.g., CH_4 and carbon monoxide (CO). The tropospheric budget of O_3 is governed by its production through the photochemical oxidation of CH_4, CO and non-methane volatile organic compounds (NMVOC) in the presence of oxides of nitrogen (NO_x); removal by several chemical reactions; removal by dry deposition at surface of the Earth; and the downward transport of O_3 from the stratosphere.

This paper extends recent work on improvements to the oceanic O_3 dry deposition parameterisation (Luhar et al., 2018) and lightning-generated NO_x (referred to as LNO_x) parameterisation (Luhar et al., 2021) to investigate the impact on radiative transfer of these improvements via the use of the global Australian Community Climate and Earth System Simulator – United

https://doi.org/10.5194/acp-2022-275
Preprint. Discussion started: 26 April 2022

Atmospheric Chemistry and Physics Discussions

Kingdom Chemistry and Aerosol (ACCESS-UKCA) chemistry-climate model. One of the primary purposes of improving these physico-chemical processes is to improve the overall performance of chemistry-climate and earth system models. Dry deposition is a significant sink of O_3 (Galbally and Roy, 1980; Luhar et al., 2017; Clifton et al., 2020), affecting O_3 mixing ratio, and its long-range transport and lifetime. The improved dry deposition parameterisation is a mechanistic air–sea exchange scheme that accounts for the concurrent waterside processes of molecular diffusion, O_3 solubility, first-order chemical reaction of O_3 with dissolved iodide, and turbulent transfer. It is a significant improvement over the assumption in most chemical transport models that the controlling term of surface resistance in the scheme for dry deposition velocity of O_3 at the ocean surface is constant based on Wesely (1989), and leads to a smaller O_3 dry deposition velocity to the ocean (by a factor of 2–3) and a larger tropospheric O_3 burden.

Although LNO_x accounts for only about 10% of the global NO_x source, it has a disproportionately large contribution to the tropospheric burdens of O_3 and the hydroxyl (OH) radical (Dahlmann et al., 2011; Murray, 2016). The impact on both O_3 and the CH_4 lifetime (against loss by tropospheric OH) in turn influences atmospheric radiative transfer. Schumann and Huntrieser (2007) report a large uncertainty range of 2–8 Tg nitrogen (N) yr^{-1} in the global amount of LNO_x generated.

As a side note, while we estimate the globally-averaged direct energy dissipated from lightning flashes to be only ~ 0.2 mW m^{-2}, the radiative energy retained in the atmosphere due to the net impact of LNO_x on O_3 production and CH_4 loss is ~ 40 mW m^{-2} per Tg N yr^{-1} produced due to lightning (see section 3.3), which implies a radiative impact of ~ 80 – 320 mW m^{-2} corresponding to the above LNO_x range, which is roughly three orders of magnitude larger than the direct energy release, a remarkable atmospheric amplifier.

The improved LNO_x parameterisation by Luhar et al. (2021) is a refinement over the widely-used lightning flash rate parameterisation developed by Price and Rind (1992) (PR92), especially for the ocean for which the PR92 parameterisation greatly underestimates the lightning flash rate and therefore results in a lower tropospheric O_3 burden.

We conduct a number of ACCESS-UKCA model simulations to quantify the effects of the above two parameterisation changes on the net downward shortwave (SW) and longwave (LW) radiative fluxes at the top of the atmosphere (TOA), and the downward surface SW and LW radiative fluxes, and these are reported here. Part of these changes arises due to the changes in atmospheric lifetime of CH_4, and that is included in the discussion. The calculated changes in the radiative fluxes are also put in the context of the IPCC anthropogenic ERF estimates.

2 The ACCESS-UKCA global chemistry-climate model and model setup

We use the United Kingdom Chemistry and Aerosol (UKCA) global atmospheric composition model (Abraham et al., 2012; https://www.ukca.ac.uk) coupled to ACCESS (Australian Community Climate and Earth System Simulator) (Bi et al., 2013; Woodhouse et al., 2015). In the simulations carried out here, ACCESS is essentially the same as the U.K. Met Office's Unified

https://doi.org/10.5194/acp-2022-275
Preprint. Discussion started: 26 April 2022


Atmospheric Chemistry and Physics Discussions

Model (UM) (vn8.4) as the ACCESS specific land-surface and ocean components are not invoked. The UM's original land-surface scheme (viz. JULES) is used and the model is run in atmosphere-only mode with prescribed monthly-mean sea surface temperature (SST) and sea ice fields. The atmosphere component of the UM vn8.4 is the Global Atmosphere (GA 4.0) (Walters et al., 2014). The UKCA configuration used here is the so-called StratTrop (or Chemistry of the Stratosphere and Troposphere (CheST)) (Archibald et al., 2020), which also includes the GLObal Model of Aerosol Processes (GLOMAP)-mode aerosol scheme (Mann et al., 2010).

The tropospheric chemistry scheme includes the chemical cycles of O_x, HO_x and NO_x, and the oxidation of CO, CH_4, and other volatile organic carbon (VOC) species (for example, ethane, propane, and isoprene). The Fast-JX photolysis scheme reported by Neu et al. (2007) and Telford et al. (2013) is used. O_3 is coupled interactively between chemistry and radiation. The aerosol section includes sulphur chemistry. The total number of chemical reactions, including those in aerosol chemistry, is 306 across 86 species.

The horizontal resolution of the atmospheric model is 1.875° longitude × 1.25° latitude, with 85 staggered terrain-following hybrid-height levels extending from the surface to 85 km in altitude (the so-called N96L85 configuration). The vertical resolution becomes coarser with height, with the lowest 65 levels (altitudes up to ~ 30 km) located within the troposphere and lower stratosphere. The model's dynamical timestep is 20 min, and the UKCA chemical solver is called every 60 min.

A global monthly-varying emissions database for reactive gases and aerosols is used, which includes both anthropogenic, biomass burning and natural components (Woodhouse et al., 2015; Desservettaz et al., 2022). Pre-2000 anthropogenic emissions are prescribed from the Atmospheric Chemistry and Climate Model Intercomparison Project (ACCMIP) (Lamarque et al., 2010), and post-2000 from Representative Concentrations Pathway (RCP) 6.0 scenario (van Vuuren et al. 2011). Biomass burning emissions are from the GFED4s database (van der Werf et al., 2017). Concentrations of CO_2, CH_4, N_2O and O_3 depleting substances are prescribed instead of emissions and are from the Coupled Model Intercomparison Project Phase 5 (CMIP5) and RCP6.0 recommendations. Biogenic emissions are from the Model of Emissions of Gases and Aerosols from Nature – Monitoring Atmospheric Composition and Climate project (MEGAN-MACC; Sindelarova et al., 2014). Details of required emissions of other species, and their original sources, including biogenic emissions, chemical precursors and primary aerosol are given by Woodhouse et al. (2015).

2.1 Model's radiation scheme for gases

ACCESS uses the broadband radiation scheme of Edwards and Slingo (1996), updated and described by Walters et al. (2014), to determine the impact of radiatively active trace gases and aerosols, including clouds, on radiative fluxes, from which heating rates and related quantities may be determined. As UKCA is coupled to this radiation scheme, it is possible calculate the radiative influence of the UKCA gaseous tracer fields (normally O_3, CH_4, N_2O and O_3 depleting substances) for any specific model configuration. In the present UKCA configuration, mixing ratios of O_3, CH_4, N_2O are coupled to the radiation code where O_3 is passed from the modelled 3-D fields.

https://doi.org/10.5194/acp-2022-275
Preprint. Discussion started: 26 April 2022


Atmospheric Chemistry and Physics Discussions

The Edwards and Slingo (1996) scheme uses the so-called correlated-k method for gaseous absorption for major gases with 6 bands in the shortwave and 9 bands in the longwave regions of the spectrum. In each spectral band, total transmission is determined by summing the results of a number of quasi-monochromatic calculations, each carried out using a two-stream approximation, in which the angular variation of the radiance field is represented simply by an upward and a downward diffuse flux, together with a direct solar flux in the shortwave region. Twenty one k terms are used for the major gases in the shortwave bands. Absorption by water vapour (H_2O), O_3, CO_2 and oxygen (O_2) is included. The treatment of O_3 absorption is as described by Zhong et al. (2008). Forty seven k terms are used for the major gases in the longwave bands. Absorption by H_2O, O_3, CO_2, CH_4, N_2O, and halocarbons is included. The treatment of CO_2 and O_3 absorption is as described by Zhong and Haigh (2000). Of the major gases considered, H_2O and O_3 are prognostic, whilst other gases are prescribed using either fixed or time-varying mass mixing ratios and assumed to be well mixed. The method of equivalent extinction (Edwards, 1996) is used for minor gases in each band.

2.2 Ozone dry deposition scheme for the ocean

Dry deposition flux of O_3 to Earth's surface is usually modelled as the product of O_3 concentration in the air near the surface and a (downward) dry deposition velocity, v_d, which is calculated as (Wesely, 1989)

$$v_d = \frac{1}{r_a + r_b + r_c}, \quad (1)$$

where r_a is the aerodynamic resistance which is the resistance to transfer by turbulence in the atmospheric surface layer, r_b is the atmospheric viscous (or quasi laminar) sublayer resistance which is the resistance to movement across a thin layer (0.1 – 1 mm) of air that is in direct contact with the surface, and r_c is the surface resistance which is the resistance to uptake by the surface itself. Various parameterisations are used to calculate these resistances. r_c is the dominant term in Eq. (1) for O_3 dry deposition to water surfaces, and it is routinely assumed that r_c for water is constant at ≈ 2000 s m^{-1} following Wesely's (1989) widely used dry deposition parameterisation. Most global chemical transport models, e.g. CAM-chem (Lamarque et al., 2012), GEOS-Chem (Mao et al., 2013) and UKCA, have followed this approach thus far by default, with ACCESS-UKCA using $r_c = 2200$ s m^{-1}.

Recently, Luhar et al. (2017, 2018) concluded that the use of the above constant r_c approach in ACCESS-UKCA overestimates O_3 deposition velocities by as much as a factor of 2 to 4 compared to measurements, and does not simulate their observed spatial variability well. Luhar et al. (2018) developed a two-layer process-based parameterisation for r_c that accounts for the concurrent waterside processes of molecular diffusion, O_3 solubility, first-order chemical reaction of O_3 with dissolved iodide, and turbulent transfer, and found that this parameterisation described the O_3 deposition velocities much better and reduced the global oceanic O_3 deposition to approximately one-third of the default value obtained using Wesely's (1989) r_c approach. Using the new parameterisation, Luhar et al. (2018) estimated an oceanic dry deposition of 98.4 ± 30.0 Tg O_3 yr^{-1} and a global

https://doi.org/10.5194/acp-2022-275
Preprint. Discussion started: 26 April 2022


Atmospheric Chemistry and Physics Discussions

one of 722.8 ± 87.3 Tg O_3 yr^{-1} (averaged over years 2003–2012), which can be compared with the respective values 340 Tg O_3 yr^{-1} and 978 ± 127 Tg O_3 yr^{-1} obtained by Hardacre et al. (2015) based on 15 global chemistry transport (for year 2001) using Wesely's scheme, demonstrating the large reduction in the oceanic value using the new parameterisation. The new approach has recently been evaluated by other researchers in both global and regional models (Loades et al., 2020; Pound et al., 2020; Barten et al., 2021).

We use both the default and new oceanic dry deposition parameterisations (the latter corresponding to the Ranking 1 configuration in Table 1 of Luhar et al. (2018)).

2.3 Lightning-generated NO_x

NO_x, which is a mixture of nitrogen dioxide (NO_2) and nitric oxide (NO), acts as a precursor to O_3 and OH, which are the principal tropospheric oxidants. The upper troposphere is where O_3 is most potent as a greenhouse gas. Lightning mainly happens in the tropics related to deep atmospheric convection and is the primary source of NO_x in the middle to upper troposphere. Schumann and Huntrieser (2007) report a range of 2 - 8 Tg nitrogen (N) yr^{-1} produced by lightning globally. The range of global LNO_x in 16 ACCMIP models in CMIP5 varied between 1.2 to 9.7 Tg N yr^{-1} (Lamarque et al., 2013), whereas in five earth system models in CMIP6 LNO_x ranged between 3.2 to 7.6 Tg N yr^{-1} (Griffiths et al., 2021; Naik et al., 2021) for the present-day (nominal year 2000) conditions.

The LNO_x amount in most global models is calculated as

$$LNO_x = P_{NO} \times F, \quad (2)$$

where P_{NO} is the quantity of NO generated per lightning flash, and F is the flash rate. F is calculated at every model time step within a model grid, and partitioned into cloud-to-ground (CG) and intracloud (IC) flash components. An emission factor of the amount of NO generated per CG/IC flash is applied, and the calculated mass of NO is then distributed vertically in the grid column (Luhar et al., 2021).

Of all the past techniques used to determine lightning flash rate in global chemistry-climate models and chemical transport models, including ACCESS-UKCA, the PR92 parameterisations are the most commonly used ones. They (or similar) have also been used in most CMIP5 and CMIP6 models.

The PR92 parameterisations for lightning flash rate (flashes per minute) over land (F_L) and ocean (F_O) are

$$F_L = 3.44 \times 10^{-5} H^{4.9}, \quad (3)$$

$$F_O = 6.4 \times 10^{-4} H^{1.73}, \quad (4)$$

https://doi.org/10.5194/acp-2022-275
Preprint. Discussion started: 26 April 2022


Atmospheric Chemistry and Physics Discussions

where H is the height of the convective cloud top (km), which is passed from the model's convective component. The above parameterisations yield flash rates over the ocean that are smaller by approximately 2 to 3 orders of magnitude compared to those calculated for clouds over land.

The oceanic parameterisation Eq. (4) is known to greatly underestimate flash rates. Recently, Luhar et al. (2021) evaluated the PR92 parameterisations and found that while the land parameterisation Eq. (3) gave satisfactory predictions, the oceanic parameterisation Eq. (4) yielded a global mean value of 0.33 flashes s^{-1} over the ocean, a much smaller value than 9.16 flashes s^{-1} obtained from satellite observations. They formulated the following improved flash-rate parameterisations using the scaling relationships between thunderstorm electrical generator power and storm geometry developed by Boccippio's (2002), together with available data:

$$F_L = 2.40 \times 10^{-5} H^{5.09}, \quad (5)$$

$$F_O = 2.0 \times 10^{-5} H^{4.38}. \quad (6)$$

Flash rates obtained using Eq. (6) are approximately two orders of magnitude greater than those obtained using Eq. (4). Eq. (5) performed very similar to Eq. (3) and the new marine parameterisation Eq. (6) gave a global mean marine flash rate of 8.84 flashes s^{-1}, which is very close to the observed value of 9.16 flashes s^{-1}.

With $P_{NO} = 330$ moles NO per flash, the use of Eqs. (5) and (6) in ACCESS-UKCA increased the mean total global LNO_x by 38% from the base value of 4.8 Tg N yr^{-1} (Luhar et al. (2021), with a corresponding increase in tropospheric O_3 burden.

We investigate the radiative effects of this change in O_3 due to the change in LNO_x.

2.4 Global model simulations

We conducted the following six ACCESS-UKCA simulations for the years 2004–2010 with O_3 and CH_4 radiation feedbacks included (except Run E). Considering the first two simulation years as model spin-up time, the output from the model for the five-year 2006–2010 was used for the analysis reported below:

- Base run (Run A): Default model run, with $r_c = 2200$ s m^{-1} in the oceanic O_3 deposition, and PR92 lightning flash rates (LNO_x = 4.8 Tg N yr^{-1}),
- Run B: New process-based oceanic O_3 deposition scheme and PR92 lightning flash rates (LNO_x = 4.8 Tg N yr^{-1}),
- Run C: New process-based oceanic O_3 deposition scheme and new lightning flash rates (LNO_x = 6.9 Tg N yr^{-1}),
- Run D: New process-based oceanic O_3 deposition scheme, and PR92 lightning flash rates but scaled to give the total global LNO_x the same as Run C (LNO_x = 6.9 Tg N yr^{-1}),
- Run E: Same as Run C, but without the CH_4 radiation feedback (to separate out the radiative effects of O_3 alone) (LNO_x = 6.9 Tg N yr^{-1}), and
- Run F: New process-based oceanic O_3 deposition scheme and LNO_x = 0.

https://doi.org/10.5194/acp-2022-275
Preprint. Discussion started: 26 April 2022

Atmospheric Chemistry and Physics Discussions

Apart from the above changes, the rest of the model setup is the same as described in Section 2 of Luhar et al. (2021). The simulations were nudged to the ECMWF's ERA-Interim reanalyses in the free troposphere involving horizontal wind components and potential temperature given on pressure levels at 6-hourly intervals (Dee et al., 2011). Each model run was initialised using a previously spun-up model output with nudging and the default lightning and dry deposition schemes. The use of nudging does not allow the model changes to adjust synoptic-scale meteorology; hence the results here represent instantaneous radiative responses in the climate system, unlike the ERF which is the sum of the instantaneous radiative forcing (IRF) and the contribution from such adjustments. Due to nudging, responses in the simulation may be dampened, but can be attributed directly to the model perturbations (Fiddes et al., 2018).

The model results were averaged over 5-years for the globe, land, sea, Northern Hemisphere and Southern Hemisphere. Differences between the base model run and the other runs were calculated were indexed as follows on x-axis in relevant plots.

- 1 (dep.) = Run B – Base
- 2 (dep. + LNO_x) = Run C – Base
- 3 (dep. + scaled LNO_x) = Run D – Base
- 4 (dep. + LNO_x + no CH_4) = Run E – Base
- 5 (dep. + no LNO_x) = Run F – Base

3 Results and discussion

Monthly-averaged model output for various radiative components and chemical species is used in the following.

3.1 Model performance for radiative fluxes

Model output for radiative components includes the incoming (or downward) TOA solar radiation ($S\downarrow_{TOA}$), outgoing (or upward) TOA longwave radiation ($L\uparrow_{TOA}$), outgoing TOA shortwave radiation ($S\uparrow_{TOA}$), incoming longwave radiation at the surface ($L\downarrow_S$), incoming shortwave radiation at the surface ($S\downarrow_S$), outgoing longwave radiation at the surface ($L\uparrow_S$), and outgoing shortwave radiation at the surface ($S\uparrow_S$). The total radiation is the sum of the longwave and shortwave components.

The net downward TOA radiative flux is

$$R^N_{TOA} = S\downarrow_{TOA} - (L\uparrow_{TOA} + S\uparrow_{TOA}), \quad (7)$$

where the superscript N signifies net (note that $S\downarrow_{TOA}$ is the same in all runs and $L\downarrow_{TOA} = 0$). Additional definitions are: the net downward TOA shortwave radiative flux $S^N_{TOA} = S\downarrow_{TOA} - S\uparrow_{TOA}$ and the net downward TOA longwave radiative flux $L^N_{TOA} = -L\uparrow_{TOA}$. The net downward longwave radiation at the surface is equal to ($L\downarrow_S - L\uparrow_S$) and net downward shortwave radiation at the surface is equal to ($S\downarrow_S - S\uparrow_S$).

https://doi.org/10.5194/acp-2022-275
Preprint. Discussion started: 26 April 2022

Atmospheric Chemistry and Physics Discussions

The modelled radiation components from the base run can be compared with the corresponding observations available from NASA's Clouds and the Earth's Radiant Energy System (CERES) EBAF (Energy Balanced and Filled) Ed4.1 dataset (https://ceres.larc.nasa.gov/data/) for the period 2006–2010 (Loeb et al., 2018; Kato et al., 2018).

The area-weighted global averaged modelled incoming $S\downarrow_{TOA}$, and all-sky outgoing $L\uparrow_{TOA}$ and $S\uparrow_{TOA}$ radiative fluxes are 341.44, 240.61 and 102.24 W m^{-2}, respectively, in close agreement with the respective observed values of 339.93, 240.10 and 99.19 W m^{-2}. The modelled incoming $L\downarrow_S$ and $S\downarrow_S$ radiative fluxes are 341.55 and 191.49 W m^{-2} compared to the observed averages of 344.57 and 186.48 W m^{-2}, respectively. The modelled outgoing $L\uparrow_S$ and $S\uparrow_S$ radiative fluxes are 400.07 and 24.83 W m^{-2} compared to the observed averages of 398.18 and 23.21 W m^{-2}, respectively. Thus, the modelled average total net downward radiation at the surface is 108.14 W m^{-2} compared to the observed value of 109.66 W m^{-2}.

The above values can also be compared with a 16-model ensemble from a CMIP5 study (Stephens et al., 2012), which gives the outgoing $L\uparrow_{TOA}$ and $S\uparrow_{TOA}$ of 238.6 and 102.2 W m^{-2}, respectively, and the incoming $L\downarrow_S$ and $S\downarrow_S$ of 339.7 and 190.3 W m^{-2}, respectively.

A comparison of the zonal-averaged modelled $L\uparrow_{TOA} + S\uparrow_{TOA}$, $L\downarrow_S$ and $S\downarrow_S$ with the corresponding CERES-EBAF data is made in Figure 3 and discussed in section 3.2.

Fiddes et al. (2018) obtained similar evaluation results for a very similar setup of ACCESS-UKCA vn8.4 for radiation components averaged over the period of 2000–2009.

3.2 Radiative effects of the parameterisation changes

Figure 1a presents a bar chart of the modelled mean (2006–2010) difference (Δ) in the area-weighted net downward TOA total radiation (ΔR^N_{TOA}) between the various runs and the base run for the globe, tropics (< |30°|), non-tropics, land, and ocean (which includes all water bodies). ΔR^N_{TOA} is akin to radiative forcing, a positive ΔR^N_{TOA} means more radiation is retained in the atmosphere due to perturbation to the base model setup. In Figure 1, the absolute values of the total outgoing TOA radiative flux ($L\uparrow_{TOA} + S\uparrow_{TOA}$) for the base run are also plotted as a reference (corresponding to the right axis). Table 1 presents values of the differences ΔR^N_{TOA}, $\Delta L\downarrow_S$ and $\Delta S\downarrow_S$ for the globe, tropics, and non-tropics. It is apparent that with the new oceanic deposition scheme, the net downward TOA radiation (R^N_{TOA}) is increased by only a relatively very small amount of 4.3 mW m^{-2}. With the new lightning flash-rate scheme this increase is much greater at 86.3 mW m^{-2} due to enhanced tropospheric O_3 production and CH_4 loss as LNO_x is increased (to 6.9 from the base value 4.8 Tg N yr^{-1}). If we turn off the radiative feedbacks of CH_4 in the model, the increase in the net downward TOA radiative flux is 107.0 mW m^{-2}. Therefore, CH_4 feedback negates the positive radiative effect of O_3 by 20.7 mW m^{-2}, which is due to enhanced OH concentrations resulting from increased LNO_x that reduce the tropospheric CH_4 lifetime and increase $L\uparrow_{TOA}$. (Note that dry deposition is a surface process and, therefore, any

https://doi.org/10.5194/acp-2022-275
Preprint. Discussion started: 26 April 2022


Atmospheric Chemistry and Physics Discussions

changes to it would influence O_3 in surface air to much greater extent than that at higher altitudes, although the radiative effects of these changes may be small.)

When the default PR92 lightning flash rate scheme is used with a uniform scaling so as to give the total global LNO_x the same as Run 3 (i.e., 6.9 Tg N yr^{-1}), the increase in the net downward TOA radiation is 70.9 mW m^{-2}. Therefore, although the total global LNO_x is the same in both runs, the new lightning flash rate scheme leads to a larger increase, which implies that how LNO_x is spatially distributed makes a difference in the radiation impact.

LNO_x is an important precursor of tropospheric O_3 and OH. Turning off LNO_x completely in the model causes an extra 190.8 mW m^{-2} to leave the atmosphere compared to the base run. This is caused by the lower amount of O_3 due to the absence of LNO_x in the atmosphere. This increase in outgoing radiation due to reduced upper tropospheric O_3 dominates over the reverse radiation impact of no LNO_x causing lower OH and a longer CH_4 lifetime.

There may be a small negative contribution to the net downward TOA radiative flux through formation of nitrate aerosols as LNO_x is increased, but most global chemistry-climate models (including ACCESS-UKCA) do not include nitrate aerosols (e.g., only three of the AerChemMIP models have this capability).

In Figure 1a, the radiation changes relative to the base run are larger in magnitude in the tropics than elsewhere. With the new oceanic deposition scheme, the net downward TOA radiation is increased by 13.7 mW m^{-2} in the tropics but is reduced by 5.5 mW m^{-2} elsewhere. The contrast in radiation changes over land the ocean is not as stark as that over the tropical and non-tropical regions, except for the no-LNO_x case.

Figure 1b and Figure 1c are the same as Figure 1a except for the differences in the net downward TOA radiation components L^N_{TOA} and S^N_{TOA}, respectively, and these suggest that when the new LNO_x scheme is used, the changes in the total net downward TOA radiation are dominated by the changes in the longwave component (L^N_{TOA}).

The magnitude of the above modelled net downward TOA radiation differences obtained due to the differences in the representation of two natural processes in the model can be put in the context of the IPCC AR6 reported anthropogenic ERF due to O_3 over the years 1750–2019 of 470 ± 230 mW m^{-2} (Forster et al., 2021), noting that the radiation differences calculated here are akin to instantaneous radiative forcing, which excludes any adjustments (e.g., adjustments causing circulation changes) unlike the ERF which is the sum of the IRF and the contribution from the adjustments. For example, the extra radiation of 86.3 mW m^{-2} retained by the atmosphere when the new deposition and lightning flash-rate schemes are used, which represents the uncertainty in radiation due to two natural process representation in chemistry-climate models, is 18% of the anthropogenic O_3 radiative forcing.

Figure 2a is a bar chart of the modelled mean difference of the area-weighted downward surface longwave radiative flux ($\Delta L{\downarrow}_S$) between the various runs and the base run. The absolute values of the surface longwave radiative flux for the base run

https://doi.org/10.5194/acp-2022-275
Preprint. Discussion started: 26 April 2022

Atmospheric Chemistry and Physics Discussions

are also plotted as a reference. Figure 2b is the corresponding plot for the downward surface shortwave radiative flux difference ($\Delta S\downarrow_S$). The LNO_x increases in the model, compared to the base run, lead to an increase in $L\downarrow_S$, and a decrease in $S\downarrow_S$.

https://doi.org/10.5194/acp-2022-275
Preprint. Discussion started: 26 April 2022

Atmospheric Chemistry and Physics Discussions

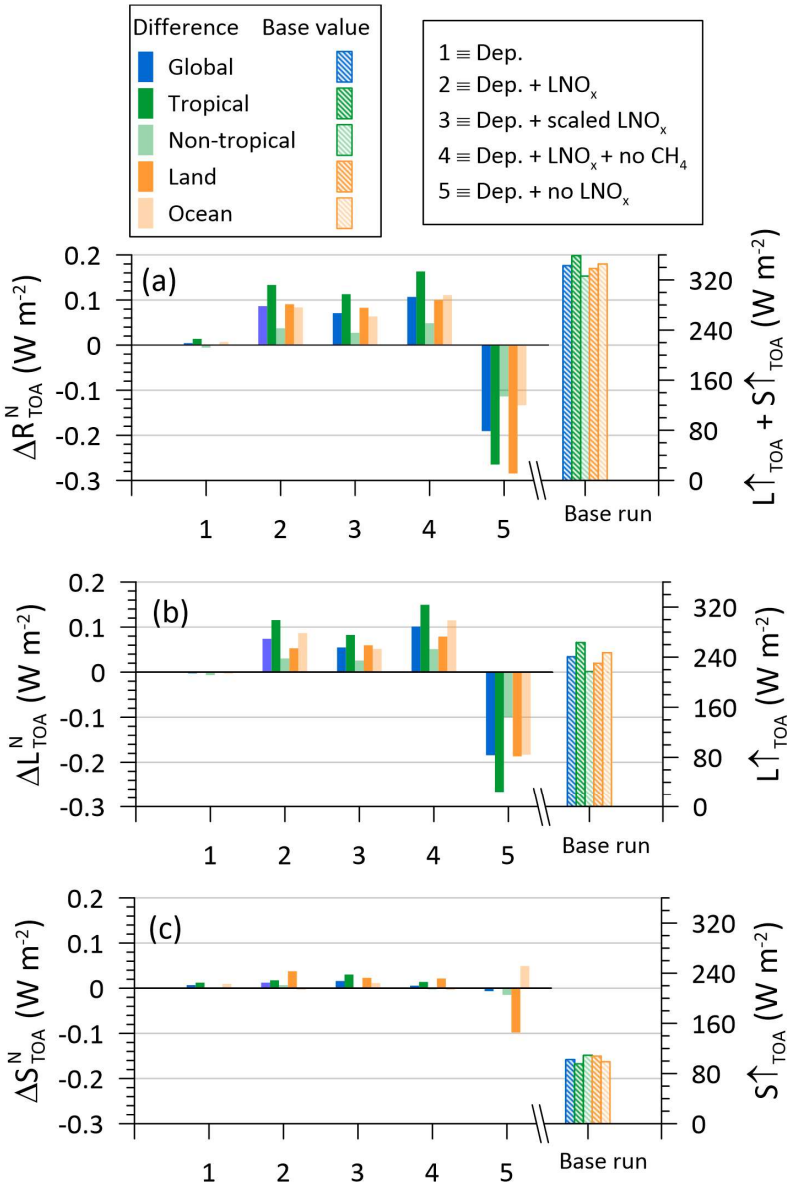

Figure 1: Modelled mean (2006–2010) net downward TOA radiative flux difference between the various model runs and the base run (1 = Run B – Base, 2 = Run C – Base, 3 = Run D – Base, 4 = Run E – Base, 5 = Run F – Base) for the globe, tropics (< |30°|), non-tropics, land, and ocean. The plots are for the (a) total radiative flux difference (ΔR^N_{TOA}), (b) longwave radiative flux difference (L^N_{TOA}), and (c) shortwave radiative flux difference (S^N_{TOA}). The outgoing TOA flux values obtained from the base run are also plotted (corresponding to the right axis).

https://doi.org/10.5194/acp-2022-275
Preprint. Discussion started: 26 April 2022

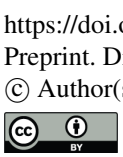

Atmospheric Chemistry and Physics Discussions

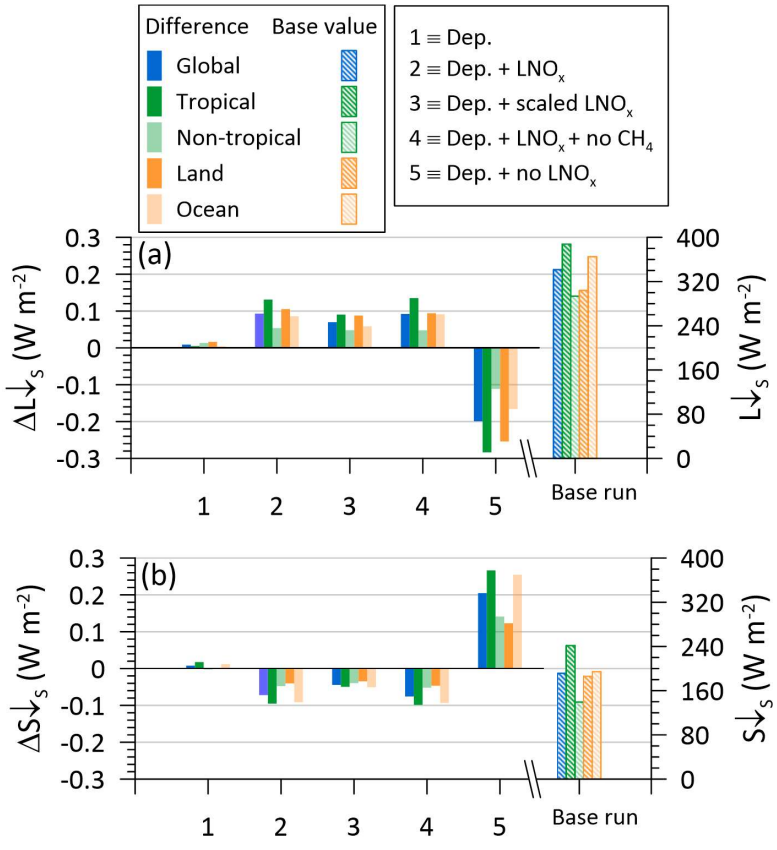

Figure 2: Modelled mean (2006–2010) downward surface radiative flux difference between the various model runs and the base run (1 = Run B – Base, 2 = Run C – Base, 3 = Run D – Base, 4 = Run E – Base, 5 = Run F – Base) for the globe, tropics (< |30°|), non-tropics, land, and sea. The plots are for the (a) longwave radiative flux difference ($\Delta L\downarrow_S$) and (b) shortwave radiative flux difference ($\Delta S\downarrow_S$). The downward surface flux ($L\downarrow_S+S\downarrow_S$) values obtained from the base run are also plotted (corresponding to the right axis).

https://doi.org/10.5194/acp-2022-275
Preprint. Discussion started: 26 April 2022

Atmospheric Chemistry and Physics Discussions

Table 1: Changes in the net downward total top-of-the-atmosphere (TOA) radiative flux (ΔR^N_{TOA}), and in the incoming longwave ($\Delta L\downarrow_S$) and shortwave ($\Delta S\downarrow_S$) fluxes at the surface, with respect to the base run. Values (mW m^{-2}) given for averages over the globe, tropics (< |30°|), and non-tropics over 2006–2010).

Model difference	Globe			Tropics			Non-tropics		
	ΔR^N_{TOA} (mW m^{-2})	$\Delta L\downarrow_S$ (mW m^{-2})	$\Delta S\downarrow_S$ (mW m^{-2})	ΔR^N_{TOA} (mW m^{-2})	$\Delta L\downarrow_S$ (mW m^{-2})	$\Delta S\downarrow_S$ (mW m^{-2})	ΔR^N_{TOA} (mW m^{-2})	$\Delta L\downarrow_S$ (mW m^{-2})	$\Delta S\downarrow_S$ (mW m^{-2})
1 (dep.)	4.3	9.0	7.8	13.7	4.7	17.7	-5.5	13.4	-2.4
2 (dep. + LNO_x)	86.3	93.1	-72.1	133.4	131.0	-95.3	37.4	53.8	-47.9
3 (dep. + scaled LNO_x)	70.9	69.7	-44.6	113.0	90.5	-49.5	27.1	48.2	-39.5
4 (dep. + LNO_x + no CH_4)	107.0	92.3	-75.6	163.2	135.1	-98.4	48.6	47.9	-51.9
5 (dep. + no LNO_x)	-190.8	-199.2	204.9	-264.8	-283.7	266.3	-114.1	-111.4	141.1

In Figure 3 (a, b and c), the zonal means of the differences in the modelled radiative fluxes from the base model run for the various other model runs for downward TOA net radiative flux, downward surface longwave radiative flux and downward surface shortwave radiative flux are presented (solid lines). The zonal means of the outgoing TOA radiative flux ($L\uparrow_{TOA}$ +$S\uparrow_{TOA}$), downward long wave radiative flux at the surface and downward short wave radiative flux at the surface from the base run, and the corresponding CERES-EBAF data, are also plotted (dotted lines and solid circles, corresponding to the right axis).

In Figure 3a, the minimum in the zonal mean of the modelled $L\uparrow_{TOA}$ +$S\uparrow_{TOA}$ flux near the equator is mostly due to the high cloud tops associated with the inter-tropical convergence zone (ITCZ), which is a region of persistent thunderstorms, and the subtropical maxima are associated with clear air over deserts and subtropical highs. The radiative flux diminishes towards the poles, with the minimum being in the southern hemisphere polar region. There is a good agreement with the CERES-EBAF data, with some model overestimation between 50°N to 50°S and underestimation within 50–70°S. In terms of the differences in net downward total top-of-the-atmosphere (TOA) radiative flux (R^N_{TOA}) from the base run, dry deposition has little effect, but increased LNO_x increases the flux from ~ 50°N to 30°S presumably due to increased emission of LW by O_3 produced by the LNO_x. Similarly, totally removing the LNO_x decreases the TOA radiative flux particularly from approximately 30°S to virtually the north pole showing a marked hemispheric asymmetry towards the northern hemisphere. This contrasts, being in the opposite hemisphere, to the asymmetric effect of LNO_x on the downward SW radiation at the surface (Figure 3c).

Downwards longwave radiation at the surface in clear sky conditions is such that 80% originates in the first 500 m of the atmosphere and the major controlling factors are humidity and temperature (Wang and Dickinson, 2013). In Figure 3b for downward long wave radiative flux at the surface, apparent are the characteristic peak in the tropics, the radiative flux

https://doi.org/10.5194/acp-2022-275
Preprint. Discussion started: 26 April 2022


Atmospheric Chemistry and Physics Discussions

diminishing poleward to a lower level in the northern polar region and to the lowest levels towards the southern hemisphere pole consistent with global climatologies (Wang and Dickinson, 2013). The model agreement with the CERES-EBAF data is excellent. In terms of the differences from the base run, dry deposition has little effect, but increased LNO_x increases the downward flux from ~ 40°N to 40°S presumably due to increased emission of LW by O_3 produced by the LNO_x. Similarly, totally removing the LNO_x decreases LW radiation particularly from ~ 40°N to 40°S. This contrasts with the asymmetric effect of LNO_x on SW radiation in Figure 3c.

The downward short wave radiative flux at the surface is affected by clouds which reflect and scatter solar radiation (see cloud climatology https://earthobservatory.nasa.gov/images/85843/cloudy-earth). In Figure 3c for downward shortwave radiative flux at the surface, apparent are the characteristic peak from overhead solar radiation in the tropics, the influence of the tropical cloud band, the radiative flux diminishing to a low level in the northern polar region presumably due to widespread cloud cover there, and diminishing fluxes in the mid latitudes of the southern hemisphere and then increasing towards the pole consistent with cloud climatologies (https://earthobservatory.nasa.gov/images/85843/cloudy-earth). The model agreement with the CERES-EBAF data is good, with some model overestimation in the tropics. In terms of the differences from the base run, dry deposition has little effect, but increased LNO_x decreases the downward flux from ~ 20°N to 60°S presumably due to increased absorption of SW by O_3 produced by the LNO_x. Similarly, totally removing the LNO_x increases SW radiation from ~ 40°N to 70°S. This illustrates the asymmetric effect of LNO_x in producing O_3 across the hemispheres and consequent asymmetric heating contribution.

Global distribution of the net downward TOA radiative flux difference (ΔR^{N}_{TOA}) between the model Run C (i.e., the new dry deposition scheme and the new LNO_x scheme; Diff. 2) and the base run (Figure 4a) is patchy with regions of both increased and decreased radiation compared to the base run, but with an overall increase. The difference in the incoming longwave radiative flux at the surface ($\Delta L{\downarrow}_S$) (Figure 4b) is positive almost everywhere over the globe, whereas that in the incoming shortwave radiative flux at the surface ($\Delta S{\downarrow}_S$) (Figure 4c) has a patchy global distribution with regions of both positive and negative values. The respective area-weighted spatial means of these differences in Figure 4a, b and c are 86.3 ± 387.3, 93.1 ± 184.1 and -72.1 ± 589.9 mW m^{-2}, where the standard deviations were obtained from area-weighted variances and their relatively large values reflect the spatial heterogeneity of the radiation response.

Figure 4d presents the corresponding difference in lightning flash density (Δf) between the two models, which shows a larger flash density predicted everywhere by the new LNO_x scheme, particularly over the ocean in the tropics (LNO_x is directly proportional to the lightning flash rate in our model). The area-weighted spatial pattern correlation (r) between Δf and ΔR^{N}_{TOA} is 0.15. The correlation of Δf with $\Delta L{\downarrow}_S$ is 0.33 and with $\Delta S{\downarrow}_S$ it is -0.14. These relatively low correlations imply that while the LNO_x production occurs (and changes from model run to run) in one spatial pattern, time is required for chemical processing from NO_x to O_3 and CH_4 and during this time advection and dispersion take place so that the radiative effects occur in a different spatial pattern.

https://doi.org/10.5194/acp-2022-275
Preprint. Discussion started: 26 April 2022

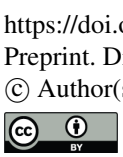

Atmospheric Chemistry and Physics Discussions

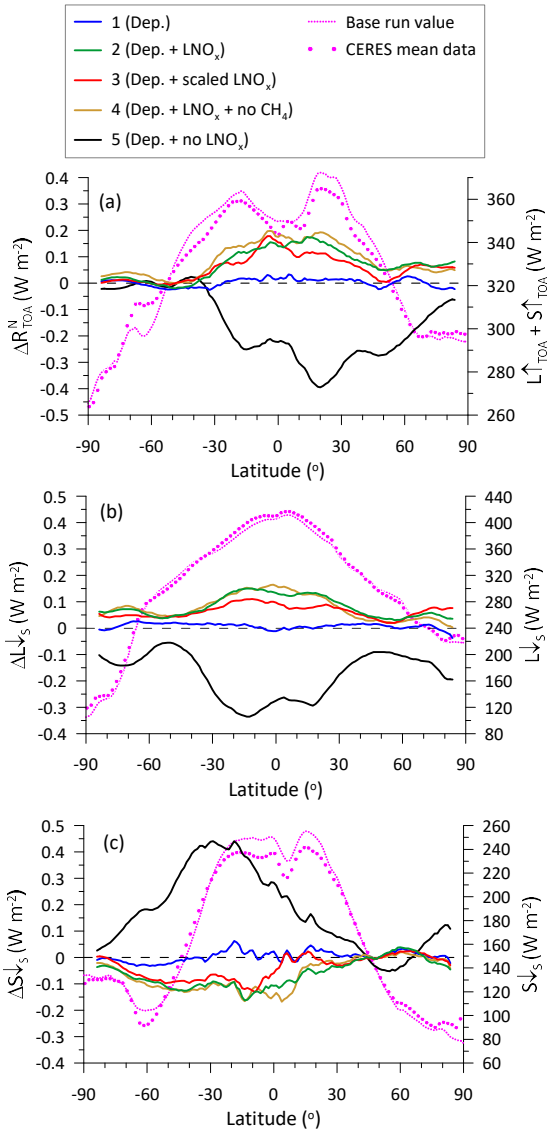

Figure 3: Zonal mean (2006–2010) of radiative flux difference between the various model runs and the base run (1 = Run B – Base, 2 = Run C – Base, 3 = Run D – Base, 4 = Run E – Base, 5 = Run F – Base). The plots (solid lines) are for the (a) net downward TOA radiative flux difference (ΔR^N_{TOA}), (b) downward longwave radiative flux difference at the surface ($\Delta L\downarrow_S$) and (b) downward shortwave radiative flux difference at the surface ($\Delta S\downarrow_S$). The solid lines are running averages (over a moving window of 10 points, i.e., 12.5°). The zonal mean flux values obtained from the base run and the corresponding CERES-EBAF data are also plotted (dotted line and solid circles, corresponding to the right axis).

https://doi.org/10.5194/acp-2022-275
Preprint. Discussion started: 26 April 2022

Atmospheric Chemistry and Physics Discussions

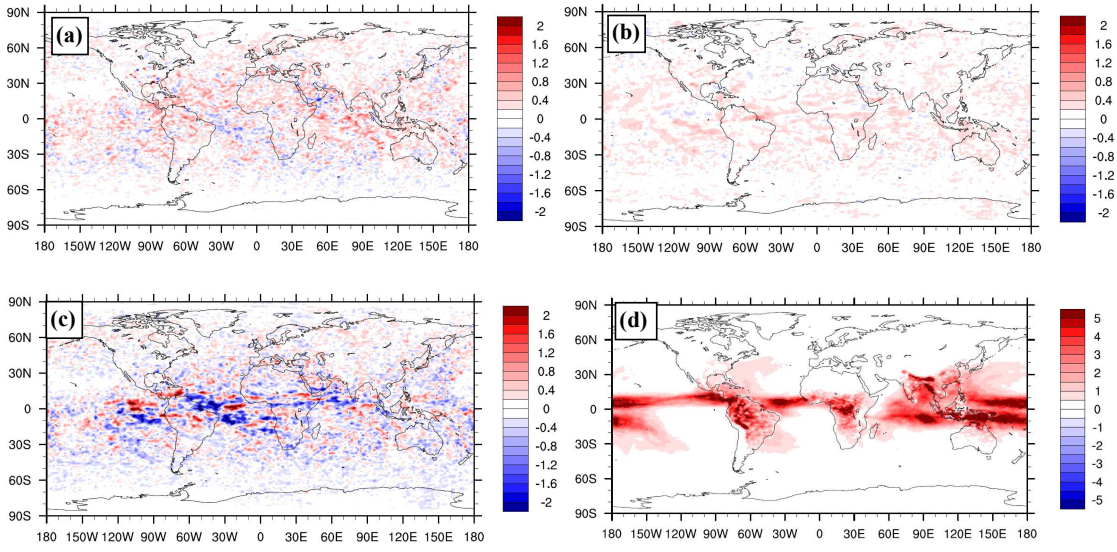

Figure 4: Global distribution of the radiative flux difference between Run C (i.e., the new dry deposition scheme and the new LNO_x scheme) and the base run (mean over 2006–2010). The plots are for the (a) net downward TOA radiative flux difference (ΔR^N_{TOA}), (b) incoming longwave radiative flux difference at the surface ($\Delta L{\downarrow}_S$) and (b) incoming shortwave radiative flux difference at the surface ($\Delta S{\downarrow}_S$). In (d), the corresponding model difference in lightning flash density, given as flashes km^{-2} yr^{-1}, is shown.

3.3 Radiative effects as a function of changes in LNO_x

Lightning NO_x production is a natural process with effects on the atmospheric radiation and energy budget via O_3, CH_4, and nitrate aerosol. Lightning NO_x is different from the bulk of other natural and anthropogenic sources of NO_x in the troposphere in that the release occurs in the upper portion of the troposphere rather than close to the Earth's surface.

In Figure 5a, we plot the change in the modelled net downward total TOA radiation (ΔR^N_{TOA}) as a function of change in the annual-averaged LNO_x production relative to the base model run. The different points are for different years and different model runs. All runs except Run E (i.e., without the CH_4 radiation feedback) are considered. The plot shows an approximately linear increasing change in the net downward total TOA radiation as a function of increase in the LNO_x production due to the various model parameterisation/configuration changes considered. (There is a relatively large gap between the LNO_x = 0 case and the LNO_x = 4.8 Tg N yr^{-1} case. To confirm that the linear fit is not unduly dominated by the LNO_x = 0 case and that the linearity is appropriate, an additional model simulation the same as Run C but with the LNO_x distribution scaled uniformly by 0.35 to give an averaged total LNO_x = 2.4 Tg N yr^{-1} was made, and the results from the this simulation are also plotted in Figure 5–Figure 6 enclosed by a dotted circle and they are included in determining the linear fits.)

https://doi.org/10.5194/acp-2022-275
Preprint. Discussion started: 26 April 2022

Atmospheric Chemistry and Physics Discussions

The slope of the best fit lines in Figure 5a suggests that with a per Tg increase in N production per year due to lightning, there is an increase of 39.6 mW m^{-2} (Tg N yr^{-1})$^{-1}$ in the net downward TOA radiation, or that much of radiation is retained by the atmosphere. Similarly, based on the slopes of the best fit lines in Figure 5b and Figure 5c, there is an increase of 40.2 mW m^{-2} (Tg N yr^{-1})$^{-1}$ in the incoming surface longwave radiation, and a decrease of 36.4 mW m^{-2} (Tg N yr^{-1})$^{-1}$ in the incoming surface shortwave radiation.

Assuming an uncertainty range of 2–8 Tg N yr^{-1} in the global estimates of lightning-generated NO_x suggested by Schumann and Huntrieser (2007), the uncertainty range in the net downward TOA radiation retained in the atmosphere due to uncertainty in LNO_x could thus be as much as 237.6 mW m^{-2} (recall that this is the net or combined radiative effect of positive O_3 and negative CH_4 feedbacks). Although these cannot be compared directly, this is equivalent to 50% of the present-day anthropogenic ERF of 470 mW m^{-2} due to O_3 over the years 1750–2019 reported by IPCC AR6 (Forster et al., 2021). The corresponding uncertainty range is 241.2 mW m^{-2} for the surface longwave radiation and 218.4 mW m^{-2} for the surface shortwave radiation. Thus, the implications of this uncertainty in LNO_x for global climate modelling needs investigation and clarification.

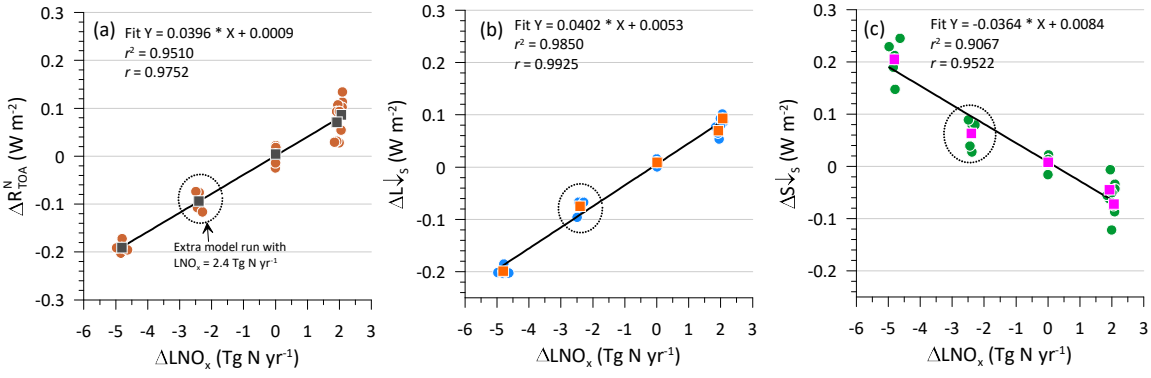

Figure 5: Change in the modelled (a) net downward total TOA radiation (ΔR^N_{TOA}), (b) incoming surface longwave radiation ($\Delta L\downarrow_S$), and (c) incoming surface shortwave radiation ($\Delta S\downarrow_S$), as a function of change in the modelled lightning-generated NO_x (ΔLNO_x, Tg N per year) relative to the Base model run. All runs except Run E (i.e., without the CH_4 radiation feedback) are considered. Results from an additional model simulation the same as Run C but with averaged LNO_x = 2.4 Tg N yr^{-1} are also plotted (enclosed in a dotted circle) to check linearity. The solid circles are the annual means whereas the squares are the mean over 2006–2010. The best fit line is based on all points.

The emission-based ERF due to increases in anthropogenic NO_x emissions (from 1750 to 2019) based on chemistry-climate models is reported to be negative (at -0.29 ± 0.29 W m^{-2}), which is a net effect of a positive ERF through enhanced tropospheric O_3 production, a negative ERF through reduced CH_4 lifetime, and a small negative ERF contribution through formation of

https://doi.org/10.5194/acp-2022-275
Preprint. Discussion started: 26 April 2022

nitrate aerosols (Naik et al., 2021). As demonstrated in this study, the net instantaneous radiative forcing of LNO_x is positive as the enhanced O_3 production dominates over the reduced CH_4 lifetime. Notwithstanding the differences between ERF and IRF, this could at least be partially because (a) in the upper to middle troposphere within which LNO_x is generated, the production efficiency of O_3 per unit of NO_x is much larger than that close to the Earth's surface, where anthropogenic emissions are mostly released (Dahlmann et al., 2011) and (b) the historical anthropogenic NO_x emissions were accompanied by emissions of reactive VOCs which affects the subsequent chemistry.

3.4 Radiative effects as a function of changes in column O_3

With the new dry deposition scheme, the tropospheric O_3 burden increases by 1.5% (by 4.2 Tg O_3 from 271.8 Tg O_3) over the base run. With both the new dry deposition and LNO_x schemes this increase in the tropospheric O_3 burden is by 11.7%. Similarly, the increase in the O_3 column is by 0.14 DU for the new dry deposition scheme and 3.75 DU for the new dry deposition and LNO_x schemes combined (from the base average total column of 304.64 DU, and the base average tropospheric column of 27.82 DU).

Radiation is examined with respect to tropospheric O_3 column changes (Figure 6). Based on Figure 6a, with a per DU increase in O_3, there is an increase of 22.8 mW m^{-2} DU^{-1} in the net downward TOA radiation, when the O_3 change is dominated by an increase in LNO_x. This can be compared to normalised radiative forcing calculations reported in the scientific literature. Using the results of 17 atmospheric chemistry models, Stevenson et al. (2013) derived a globally averaged normalized radiative forcing of 42 (range 36–45) mW m^{-2} DU^{-1} for tropospheric O_3 increase from preindustrial (1750) to present day (2010). Gauss et al. (2003) calculated a normalized radiative forcing of 36 ± 3 mW m^{-2} DU^{-1} due to changes in tropospheric O_3 between 2000 and 2100 based on the results of 11 models. In our study, the changes in TOA radiative effects per DU, which are primarily driven by changes in LNO_x parameterisation and to a much lesser extend by the O_3 deposition parameterisation (with CH_4 feedbacks included), are about half the radiative forcing per DU as a result of climate-scale changes in tropospheric O_3 (e.g., due to changes in precursor emissions and temperature). The climate-scale changes in radiation due to O_3 are larger, possibly because there are co-emissions of non-NO_x precursor species (e.g., CH_4 and VOCs) and their feedbacks, whereas in the present case only LNO_x and O_3 dry deposition changes are considered (together with CH_4 feedbacks). Methane levels and VOC emissions are unchanged.

Similarly, based on Figure 6b and Figure 6c, there is an increase in downward surface longwave radiation $L{\downarrow}_S$ by 23.6 mW m^{-2} DU^{-1} and a decrease in downward surface shortwave radiation $S{\downarrow}_S$ by 21.7 mW m^{-2} DU^{-1}.

https://doi.org/10.5194/acp-2022-275
Preprint. Discussion started: 26 April 2022

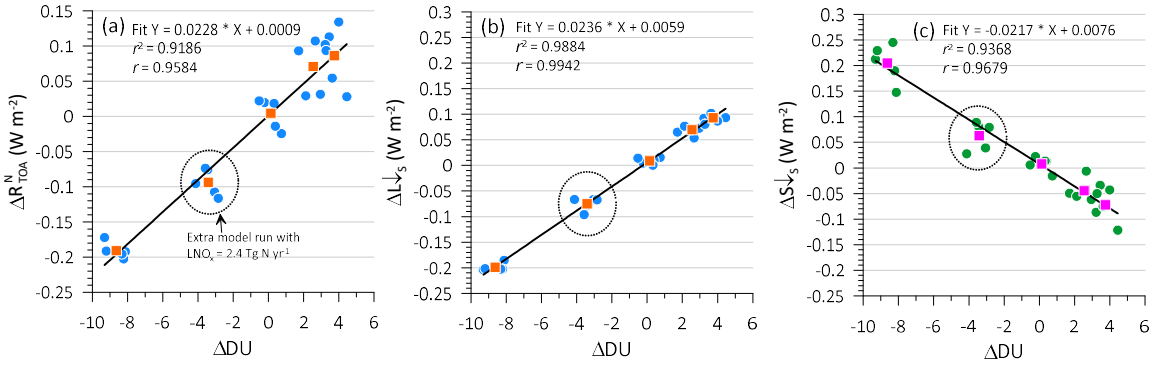

Figure 6: Change in the modelled (a) net downward total TOA radiation (ΔR^{N}_{TOA}), (b) incoming surface longwave radiation ($\Delta L{\downarrow}_S$) and (c) incoming surface shortwave radiation ($\Delta S{\downarrow}_S$), as a function of change in the modelled tropospheric O_3 column (ΔDU) relative to the Base model run. All runs except Run E (i.e., without the CH_4 radiation feedback) are considered. Results from an additional model simulation the same as Run C but with averaged LNO_x = 2.4 Tg N yr^{-1} are also plotted (enclosed in a dotted circle) to check linearity. The solid circles are the annual means whereas the squares are the mean over 2006–2010. The best fit line is based on all points.

The above changes in radiation were also examined as a function of changes in tropospheric O_3 burden (plots not shown). The slopes of these plots indicate that there is an increase of 3.3 mW m^{-2} (Tg O_3)$^{-1}$ in the net downward TOA radiation, an increase of 3.3 mW m^{-2} (Tg O_3)$^{-1}$ in the incoming surface longwave radiation, and a decrease of 3.1 mW m^{-2} (Tg O_3)$^{-1}$ in the incoming surface shortwave radiation.

In this paper, we have not explored atmospheric temperature response or any changes in atmospheric heating rates caused by the changes in the radiation balance due to the use of the improved parameterisations.

3.5 LNO_x and the tropospheric lifetime of CH_4

LNO_x also affects the lifetime of CH_4 due to loss by OH (τ_{CH_4}) in the troposphere (Labrador et al., 2004). τ_{CH_4} from Runs A, B, C, D, E and F are 7.61, 7.55, 6.97, 7.17, 6.97 and 9.26 years, respectively. Compared with the previous parameterisations, there is a relatively small decrease of 0.06 years in τ_{CH_4} when the new oceanic O_3 dry deposition scheme is used and this decrease is 0.64 years when the improved LNO_x parameterisation is also used.

In Figure 7, the change in τ_{CH_4} plotted as a function of change in LNO_x suggests that there is a shortening of the global mean CH_4 lifetime by 0.31 years per Tg N yr^{-1} produced due to lightning This change in τ_{CH_4} is equivalent to a change of –4.4% τ_{CH_4} per Tg N yr^{-1} produced due to lightning (with respect to the Run C value of τ_{CH_4}), which is close to the average –4.8 (range –6.8 to –2.4) % τ_{CH_4} per Tg N yr^{-1} given by Thornhill et al. (2021) based on four other models. The change in

https://doi.org/10.5194/acp-2022-275
Preprint. Discussion started: 26 April 2022

Atmospheric Chemistry and Physics Discussions

τ_{CH_4} corresponding to an LNO_x uncertainty range of 2–8 Tg N yr^{-1} (Schumann and Huntrieser, 2007) would be 1.9 years or 27%.

Thus, LNO_x has, through OH, a significant influence on the atmospheric lifetime of CH_4, and the value of LNO_x used within a model will influence the time integrated measures of radiative forcing including the ERF and the global warming potential of anthropogenic CH_4. The accepted atmospheric lifetime of CH_4 due to reaction with OH, soil removal and stratospheric oxidation is 7.8 years (average over 2000–2009) with a range of 6.5–8.8 years (Saunois et al., 2020). If the intermediate relationships are linear, then the uncertainty in LNO_x within the models would translate to an uncertainty of ±16% in the integrated measures of radiative forcing including the ERF and the GWP of anthropogenic CH_4.

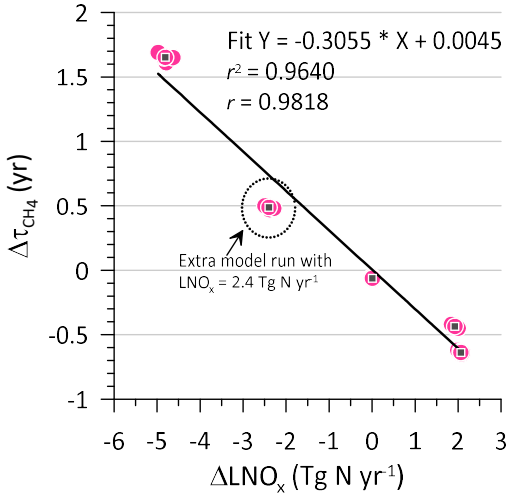

Figure 7: Same as Figure 5, except for change in the modelled CH_4 lifetime ($\Delta\tau_{CH_4}$).

4 Conclusions

The impact of recently improved global parameterisations of oceanic O_3 dry deposition (Luhar et al., 2018) and lightning-generated NO_x (Luhar et al., 2021) on radiative transfer was investigated via the use of the ACCESS-UKCA chemistry-climate model involving radiative feedbacks of both O_3 and CH_4. The main radiation components examined were the net downward top of the atmosphere (TOA) radiative flux, and the incoming longwave and shortwave radiation at the Earth's surface.

The use of the new oceanic dry deposition scheme resulted in a relatively small increase of 4.3 mW m^{-2} in the net downward TOA radiative flux, but this increase was much larger at 86.3 mW m^{-2}, most of which longwave, when the improved LNO_x

https://doi.org/10.5194/acp-2022-275
Preprint. Discussion started: 26 April 2022

Atmospheric Chemistry and Physics Discussions

parameterisation was also used (the latter increased the global LNO_x production to 6.9 from 4.8 Tg N yr^{-1}). This radiative flux difference is a net effect (107.0 - 20.7 mW m^{-2}) of an increase in O_3 and a decrease in CH_4 lifetime (by 0.64 years) against loss due to an increase in OH. It represents a measure of uncertainty in radiation due to two natural process representation in chemistry-climate models, and, for comparison, is equivalent to ~18% of the IPCC AR6 reported present-day anthropogenic radiative forcing due to O_3.

Similarly, there was an increase of 93 mW m^{-2} in the downward longwave radiation and a decrease of 72 mW m^{-2} in the downward shortwave radiation at the Earth's surface. The changes in radiation components and CH_4 lifetime per unit change in LNO_x and column O_3 were also estimated based on the slopes of linear fits.

The uncertainty range in the net downward TOA radiative flux due to the uncertainty in global estimates of LNO_x could be as much as 238 mW m^{-2}. This value is equivalent to 50% of the present-day anthropogenic radiative forcing due to O_3 of 470 mW m^{-2} reported by IPCC AR6. The corresponding modelled uncertainty range is 241 mW m^{-2} for the surface longwave radiation and 218 mW m^{-2} for the surface shortwave radiation.

The radiation changes due to the two improved parameterisations were larger in magnitude in the tropics than elsewhere. It was also found that when the default PR92 lightning flash rate scheme was used with a uniform scaling so as to give the total global LNO_x the same as the new scheme, the new scheme yielded a larger net downward TOA radiation by ~15 mW m^{-2}, which implies that how LNO_x is distributed spatially makes a difference to how the radiative transfer is impacted.

Clearly, the impact of LNO_x on the tropospheric O_3 production and oxidising capacity is considerable, with ramifications on Earth's radiation budget. Similarly, LNO_x has a significant influence on the atmospheric lifetime of CH_4, and the value of LNO_x used within a model may influence the modelled ERF of anthropogenic CH_4. Recent chemistry-climate modelling studies have explored changes in LNO_x in a future warming climate but there remains a large uncertainty depending on how lightning flash-rate parameterisations are formulated. All CMIP6 Earth system models use flash-rate parameterizations that use convective cloud-top height (as is the case in the present paper) and they project an increase in lightning and hence in LNO_x in a warmer world of 0.27–0.61 Tg N yr^{-1} per °C (Naik et al., 2021; Thornhill et al., 2021). Finney et al. (2018) find that a flash-rate parameterisation based on upward cloud ice flux predicts a decrease in lightning under climate change. Thus, despite the improvements in understanding, LNO_x remains a significant uncertainty for climate and earth system modelling.

Data availability

We used the following sources of the observational datasets for the present study: ERA-Interim global reanalysis data from https://www.ecmwf.int/en/forecasts/datasets/reanalysis-datasets/era-interim. Radiation data used for model comparison purposes were available from NASA's Clouds and the Earth's Radiant Energy System (CERES) EBAF (Energy Balanced and

https://doi.org/10.5194/acp-2022-275
Preprint. Discussion started: 26 April 2022


Atmospheric Chemistry and Physics Discussions

Filled) Ed4.1 dataset (https://ceres.larc.nasa.gov/data/). The global model output (in NetCDF) from the ACCESS-UKCA simulations made can be obtained by contacting the corresponding author (Ashok Luhar: ashok.luhar@csiro.au).

Author contributions

All authors had the initial idea to carry out this work. AKL designed the study, performed the model simulations, analysed model output and data, and prepared the manuscript. IEG co-designed the study, advised on various components of the paper, and contributed to paper writing. MTW advised on model setup. All authors contributed to revisions of the paper.

Competing interests

The authors declare that they have no conflict of interest.

Acknowledgements

This work was partly supported by the Climate Systems Hub of the National Environmental Science Program (NESP) funded by the Australian Government, and was undertaken with the assistance of resources and services from the National Computational Infrastructure (NCI), which is supported by the Australian government. ERA-Interim data from the European Centre for Medium-Range Weather Forecasts (ECMWF) and radiation data from NASA's Clouds and the Earth's Radiant Energy System (CERES) were used in this research. We acknowledge Martin Dix for his help with model configuration issues.

https://doi.org/10.5194/acp-2022-275
Preprint. Discussion started: 26 April 2022

Atmospheric Chemistry and Physics Discussions

References

Abraham, N. L., Archibald, A. T., Bellouin, N., Boucher, O., Braesicke, P., Bushell, A., Carslaw, K. S., Collins, W., Dalvi, M., Emmerson, K. M., Folberth, G., Haywood, J., Johnson, C., Kipling, Z., Macintyre, H., Mann, G. W., Telford, P. J., Merikanto, J., Morgenstern, O., O'Connor, F., Ordonez, C., Osprey, S., Pringle, K. J., Pyle, J. A., Rae, J. G. L., Reddington, C. L., Savage, D., Spracklen, D., Stier, P., and West, R.: Unified Model Documentation Paper No. 84 (http://www.ukca.ac.uk/images/b/b1/Umdp_084-umdp84.pdf): United Kingdom Chemistry and Aerosol (UKCA) Technical Description MetUM Version 8.4. UK Met Office, Exeter (UK), pp. 74, 2012.

Archibald, A. T., O'Connor, F. M., Abraham, N. L., Archer-Nicholls, S., Chipperfield, M. P., Dalvi, et al.: Description and evaluation of the UKCA stratosphere–troposphere chemistry scheme (StratTrop vn 1.0) implemented in UKESM1, Geosci. Model Dev., 13, 1223–1266, https://doi.org/10.5194/gmd-13-1223-2020, 2020.

Barten, J. G. M., Ganzeveld, L. N., Steeneveld, G.-J., and Krol, M. C.: Role of oceanic ozone deposition in explaining temporal variability in surface ozone at High Arctic sites, Atmos. Chem. Phys., 21, 10229–10248, https://doi.org/10.5194/acp-21-10229-2021, 2021.

Bi, D. H., Dix, M., Marsland, S. J., O'Farrell, S., Rashid, H. A., Uotila, P., Hirst, A. C., Kowalczyk, E., Golebiewski, M., Sullivan, A., Yan, H. L., Hannah, N., Franklin, C., Sun, Z. A., Vohralik, P., Watterson, I., Zhou, X. B., Fiedler, R., Collier, M., Ma, Y. M., Noonan, J., Stevens, L., Uhe, P., Zhu, H. Y., Griffies, S. M., Hill, R., Harris, C., and Puri, K.: The ACCESS coupled model: description, control climate and evaluation, Australian Meteorological and Oceanographic Journal, 63, 41–64, https://doi.org/10.22499/2.6301.004, 2013.

Boccippio, D. J.: Lightning scaling relations revisited, J. Atmos. Sci., 59, 1086–1104, https://doi.org/10.1175/1520-0469(2002)059<1086:LSRR>2.0.CO;2, 2002.

Clifton, O. E., Fiore, A. M., Massman, W. J., Baublitz, C. B., Coyle, M., Emberson, L., et al.: Dry deposition of ozone over land: processes, measurement, and modelling, Reviews of Geophysics, 58, e2019RG000670, https://doi.org/10.1029/2019RG000670, 2020.

Dahlmann, K., Grewe, V., Ponater, M., and Matthes, S.: Quantifying the contributions of individual NO_x sources to the trend in ozone radiative forcing, Atmos. Environ., 45, 2860–2868, https://doi.org/10.1016/j.atmosenv.2011.02.071, 2011.

Dee, D. P., Uppala, S. M., Simmons, A. J., Berrisford, P., Poli, P., Kobayashi, S., Andrae, U., Balmaseda, M. A., Balsamo, G., Bauer, P., Bechtold, P., Beljaars, A. C. M., van de Berg, L., Bidlot, J., Bormann, N., Delsol, C., Dragani, R., Fuentes, M., Geer, A. J., Haimberger, L., Healy, S. B., Hersbach, H., Holm, E. V., Isaksen, L., Kallberg, P., Kohler, M., Matricardi, M., McNally, A. P., Monge-Sanz, B. M., Morcrette, J.-J., Park, B.-K., Peubey, C., de Rosnay, P., Tavolato, C., Thepaut, J.-N., and Vitarta, F.: The ERA-Interim reanalysis: configuration and performance of the data assimilation system, Q. J. Roy. Meteor. Soc., 137, 553–597, https://doi.org/10.1002/qj.828, 2011.

https://doi.org/10.5194/acp-2022-275
Preprint. Discussion started: 26 April 2022

Atmospheric Chemistry and Physics Discussions

Desservettaz, M. J., Fisher, J. A., Luhar, A. K., Woodhouse, M. T., Bukosa, B., Buchholz, R. R., et al.: Australian fire emissions of carbon monoxide estimated by global biomass burning inventories: Variability and observational constraints, Journal of Geophysical Research: Atmospheres, 127, e2021JD035925, https://doi.org/10.1029/2021JD035925, 2022.

Edwards, J. M.: Efficient calculation of infrared fluxes and cooling rates using the two-stream equations, J. Atmos. Sci., 53, 1921–1932, https://doi.org/10.1175/1520-0469(1996)053<1921:ECOIFA>2.0.CO;2, 1996.

Edwards, J. M. and Slingo, A.: Studies with a flexible new radiation code. I: Choosing a configuration for a large-scale model, Q. J. Roy. Meteorol. Soc., 122, 689–719, https://doi.org/10.1002/qj.49712253107, 1996.

Fiddes, S. L., Woodhouse, M. T., Nicholls, Z., Lane, T. P., and Schofield, R.: Cloud, precipitation and radiation responses to large perturbations in global dimethyl sulfide, Atmos. Chem. Phys., 18, 10177–10198, https://doi.org/10.5194/acp-18-10177-2018, 2018.

Finney, D. L., Doherty, R. M., Wild, O., Stevenson, D. S., MacKenzie, I. A., and Blyth, A. M.: A projected decrease in lightning under climate change, Nat. Clim. Change, 8, 210–213, https://doi.org/10.1038/s41558-018-0072-6, 2018.

Forster, P., Storelvmo, T., Armour, K., Collins, W., Dufresne, J. L., Frame, D., Lunt, D. J., Mauritsen, T., Palmer, M. D., Watanabe, M., Wild, M., Zhang, H.: The Earth's Energy Budget, Climate Feedbacks, and Climate Sensitivity. In: Climate Change 2021: The Physical Science Basis. Contribution of Working Group I to the Sixth Assessment Report of the Intergovernmental Panel on Climate Change [Masson-Delmotte, V., Zhai, P., Pirani, A., Connors, S. L., Péan, C., Berger, S., Caud, N., Chen, Y., Goldfarb, L., Gomis, M. I., Huang, M., Leitzell, K., Lonnoy, E., Matthews, J. B. R., Maycock, T. K., Waterfield, T., Yelekçi, O., Yu, R., and Zhou, B. (eds.)]. Cambridge University Press. In Press, 2021.

Galbally, I. E. and Roy, C. R.: Destruction of ozone at the Earth's surface, Q. J. Roy. Meteor. Soc., 106, 599–620, https://doi.org/10.1002/qj.49710644915 1980.

Gauss, M., Myhre, G., Pitari, G., Prather, M. J., Isaksen, I. S. A., Berntsen, T. K., Brasseur, G. P., Dentener, F. J., Derwent, R. G., Hauglustaine, D. A., Horowitz, L. W., Jacob, D. J., Johnson, M., Law, K. S., Mickley, L. J., Muller, J.-F., Plantevin, P.-H., Pyle, J. A., Rogers, H. L., Stevenson, D. S., Sundet, J. K., van Weele, M., and Wild, O.: Radiative forcing in the 21st century due to ozone changes in the troposphere and the lower stratosphere, J. Geophys. Res., 108, 4292, https://doi.org/10.1029/2002JD002624, 2003.

Griffiths, P. T., Murray, L. T., Zeng, G., Shin, Y. M., Abraham, N. L., Archibald, A. T., Deushi, M., Emmons, L. K., Galbally, I. E., Hassler, B., Horowitz, L. W., Keeble, J., Liu, J., Moeini, O., Naik, V., O'Connor, F. M., Oshima, N., Tarasick, D., Tilmes, S., Turnock, S. T., Wild, O., Young, P. J., and Zanis, P.: Tropospheric ozone in CMIP6 simulations, Atmos. Chem. Phys., 21, 4187–4218, https://doi.org/10.5194/acp-21-4187-2021, 2021.

Kato, S., Rose, F. G., Rutan, D. A., Thorsen, T. E., Loeb, N. G., Doelling, D. R., Huang, X., Smith, W. L., Su, W., and Ham, S.-H.: Surface irradiances of Edition 4.0 Clouds and the Earth's Radiant Energy System (CERES) Energy Balanced and Filled (EBAF) data product, Journal of Climate, 31, 4501-4527, https://doi.org/10.1175/JCLI-D-17-0523.1, 2018.

Labrador, L. J., von Kuhlmann, R., and Lawrence, M. G.: Strong sensitivity of the global mean OH concentration and the tropospheric oxidizing efficiency to the source of NO_x from lightning, Geophysical Research Letters, 31, L06102, https://doi.org/10.1029/2003GL019229, 2004.

Lamarque, J.-F., Bond, T. C., Eyring, V., Granier, C., Heil, A., Klimont, Z., Lee, D., Liousse, C., Mieville, A., Owen, B., Schultz, M. G., Shindell, D., Smith, S. J., Stehfest, E., Van Aardenne, J., Cooper, O. R., Kainuma, M., Mahowald, N., McConnell, J. R., Naik, V., Riahi, K., and van Vuuren, D. P.: Historical (1850–2000) gridded anthropogenic and biomass burning emissions of reactive gases and aerosols: methodology and application, Atmos. Chem. Phys., 10, 7017–7039, https://doi.org/10.5194/acp-10-7017-2010, 2010.

Lamarque, J.-F., Emmons, L. K., Hess, P. G., Kinnison, D. E., Tilmes, S., Vitt, F., Heald, C. L., Holland, E. A., Lauritzen, P. H., Neu, J., Orlando, J. J., Rasch, P. J., and Tyndall, G. K.: CAM-chem: description and evaluation of interactive at mospheric chemistry in the Community Earth System Model, Geosci. Model Dev., 5, 369–411, https://doi.org/10.5194/gmd-5-369-2012, 2012.

Lamarque, J.-F., Shindell, D. T., Josse, B., Young, P. J., Cionni, I., Eyring, V., Bergmann, D., Cameron-Smith, P., Collins, W. J., Doherty, R., Dalsoren, S., Faluvegi, G., Folberth, G., Ghan, S. J., Horowitz, L. W., Lee, Y. H., MacKenzie, I. A., Nagashima, T., Naik, V., Plummer, D., Righi, M., Rumbold, S. T., Schulz, M., Skeie, R. B., Stevenson, D. S., Strode, S., Sudo, K., Szopa, S., Voulgarakis, A., and Zeng, G.: The Atmospheric Chemistry and Climate Model Intercomparison Project (ACCMIP): overview and description of models, simulations and climate diagnostics, Geosci. Model Dev., 6, 179–206, https://doi.org/10.5194/gmd-6-179-2013, 2013.

Loades, D. C., Yang, M., Bell, T. G., Vaughan, A. R., Pound, R. J., Metzger, S., Lee, J. D., and Carpenter, L. J.: Ozone deposition to a coastal sea: comparison of eddy covariance observations with reactive air–sea exchange models, Atmos. Meas. Tech., 13, 6915–6931, https://doi.org/10.5194/amt-13-6915-2020, 2020.

Loeb, N. G., Doelling, D. R., Wang, H., Su, W., Nguyen, C., Corbett, J. G., Liang, L., Mitrescu, C., Rose, F. G., and Kato, S.: Clouds and the Earth's radiant energy system (CERES) energy balanced and filled (EBAF) top-of-atmosphere (TOA) edition-4.0 data product, Journal of Climate, 31, 895-918. https://doi.org/10.1175/JCLI-D-17-0208.1, 2018.

Luhar, A. K., Galbally, I. E., Woodhouse, M. T., and Thatcher, M.: An improved parameterisation of ozone dry deposition to the ocean and its impact in a global climate-chemistry model, Atmos. Chem. Phys., 17, 3749–3767, https://doi.org/10.5194/acp-17-3749-2017, 2017.

Luhar, A. K., Woodhouse, M. T., and Galbally, I. E.: A revised global ozone dry deposition estimate based on a new two-layer parameterisation for air–sea exchange and the multi-year MACC composition reanalysis, Atmos. Chem. Phys., 18, 4329–4348, https://doi.org/10.5194/acp-18-4329-2018, 2018.

Luhar, A. K., Galbally, I. E., Woodhouse, M. T., and Abraham, N. L.: Assessing and improving cloud-height-based parameterisations of global lightning flash rate, and their impact on lightning-produced NO_x and tropospheric composition in a chemistry–climate model, Atmos. Chem. Phys., 21, 7053–7082, https://doi.org/10.5194/acp-21-7053-2021, 2021.

Mann, G. W., Carslaw, K. S., Spracklen, D. V., Ridley, D. A., Manktelow, P. T., Chipperfield, M. P., Pickering, S. J., and Johnson, C. E.: Description and evaluation of GLOMAP-mode: a modal global aerosol microphysics model for the UKCA composition-climate model, Geosci. Model Dev., 3, 519–551, https://doi.org/10.5194/gmd-3-519-2010, 2010.

Mao, J., Paulot, F., Jacob, D. J., Cohen, R. C., Crounse, J. D., Wennberg, P. O., Keller, C. A., Hudman, R. C., Barkley, M. P., and Horowitz, L. W.: Ozone and organic nitrates over the eastern United States: Sensitivity to iso prene chemistry, J. Geophys. Res.-Atmos., 118, 11256–11268, https://doi.org/10.1002/jgrd.50817, 2013.

Murray, L. T.: Lightning NO_x and impacts on air quality, Current Pollution Reports, 2, 115–133, https://doi.org/10.1007/s40726-016-0031-7, 2016.

Neu, J. L., Prather, M. J., and Penner, J. E.: Global atmospheric chemistry: Integrating over fractional cloud cover, J. Geophys. Res., 112, D11306, https://doi.org/10.1029/2006JD008007, 2007.

Naik, V., Szopa, S., Adhikary, B., Artaxo, P., Berntsen, T., Collins, W. D., Fuzzi, S., Gallardo, L., Kiendler Scharr, A., Klimont, Z., Liao, H., Unger, N., Zanis, P.: Short-Lived Climate Forcers. In: Climate Change 2021: The Physical Science Basis. Contribution of Working Group I to the Sixth Assessment Report of the Intergovernmental Panel on Climate Change [Masson-Delmotte, V., Zhai, P., Pirani, A., Connors, S. L., Péan, C., Berger, S., Caud, N., Chen, Y., Goldfarb, L., Gomis, M. I., Huang, M., Leitzell, K., Lonnoy, E., Matthews, J. B. R., Maycock, T. K., Waterfield, T., Yelekçi, O., Yu, R., and Zhou, B. (eds.)]. Cambridge University Press. In Press, 2021.

Pound, R. J., Sherwen, T., Helmig, D., Carpenter, L. J., and Evans, M. J.: Influences of oceanic ozone deposition on tropospheric photochemistry, Atmos. Chem. Phys., 20, 4227–4239, https://doi.org/10.5194/acp-20-4227-2020, 2020.

Price, C. and Rind, D.: A simple lightning parameterization for calculating global lightning distributions, J. Geophys. Res.-Atmos., 97, 9919–9933, https://doi.org/10.1029/92JD00719, 1992.

Saunois, M., Stavert, A. R., Poulter, B., Bousquet, P., Canadell, J. G., Jackson, R. B., et al.: The global methane budget 2000–2017, Earth System Science Data, 12, 1561–1623, https://doi.org/10.5194/essd-12-1561-2020, 2020.

Schumann, U. and Huntrieser, H.: The global lightning-induced nitrogen oxides source, Atmos. Chem. Phys., 7, 3823–3907, https://doi.org/10.5194/acp-7-3823-2007, 2007.

Sindelarova, K., Granier, C., Bouarar, I., Guenther, A., Tilmes, S., Stavrakou, T., Müller, J.-F., Kuhn, U., Stefani, P., and Knorr, W.: Global data set of biogenic VOC emissions calculated by the MEGAN model over the last 30 years, Atmos. Chem. Phys., 14, 9317–9341, https://doi.org/10.5194/acp-14-9317-2014, 2014.

Stephens, G. L., Li, J., Wild, M., Clayson, C. A., Loeb, N. G., Kato, S., L'Ecuyer, T., Stackhouse, P. W., Lebsock, M., and Andrews, T.: An update on Earth's energy balance in light of the latest global observations, Nat. Geosci., 5, 691–696, https://doi.org/10.1038/ngeo1580, 2012.

Stevenson, D. S., Young, P. J., Naik, V., Lamarque, J.-F., Shindell, D. T., Voulgarakis, A., Skeie, R. B. et al.: Tropospheric ozone changes, radiative forcing and attribution to emissions in the Atmospheric Chemistry and Climate Model Intercomparison Project (ACCMIP), Atmos. Chem. Phys., 13, 3063–3085, https://doi.org/10.5194/acp-13-3063-2013, 2013.

Telford, P. J., Abraham, N. L., Archibald, A. T., Braesicke, P., Dalvi, M., Morgenstern, O., O'Connor, F. M., Richards, N. A. D., and Pyle, J. A.: Implementation of the Fast-JX Photolysis scheme (v6.4) into the UKCA component of the MetUM chemistry-climate model (v7.3), Geosci. Model Dev., 6, 161–177, https://doi.org/10.5194/gmd-6-161-2013, 2013.

Thornhill, G., Collins, W., Olivié, D., Skeie, R. B., Archibald, A., Bauer, S., Checa-Garcia, R., Fiedler, S., Folberth, G., Gjermundsen, A., Horowitz, L., Lamarque, J.-F., Michou, M., Mulcahy, J., Nabat, P., Naik, V., O'Connor, F. M., Paulot, F., Schulz, M., Scott, C. E., Séférian, R., Smith, C., Takemura, T., Tilmes, S., Tsigaridis, K., and Weber, J.: Climate-driven chemistry and aerosol feedbacks in CMIP6 Earth system models, Atmos. Chem. Phys., 21, 1105–1126, https://doi.org/10.5194/acp-21-1105-2021, 2021.

van der Werf, G. R., Randerson, J. T., Giglio, L., van Leeuwen, T. T., Chen, Y., Rogers, B. M., Mu, M., van Marle, M. J. E., Morton, D. C., Collatz, G. J., Yokelson, R. J., and Kasibhatla, P. S.: Global fire emissions estimates during 1997–2016, Earth Syst. Sci. Data, 9, 697–720, https://doi.org/10.5194/essd-9-697-2017, 2017.

van Vuuren, D. P., Edmonds, J., Kainuma, M., Riahi, K., Thomson, A., Hibbard, K., Hurtt, G. C., Kram, T., Krey, V., Lamarque, J. F., Masui, T., Meinshausen, M., Nakicenovic, N., Smith, S. J., and Rose, S. K.: The representative concentration pathways: An overview, Climatic Change, 109, 5–31, https://doi.org/10.1007/s10584-011-0148-z, 2011.

Walters, D. N., Williams, K. D., Boutle, I. A., Bushell, A. C., Edwards, J. M., Field, P. R., Lock, A. P., Morcrette, C. J., Stratton, R. A., Wilkinson, J. M., Willett, M. R., Bellouin, N., Bodas-Salcedo, A., et al.: The Met Office Unified Model Global Atmosphere 4.0 and JULES Global Land 4.0 configurations, Geosci. Model Dev., 7, 361–386, https://doi.org/10.5194/gmd-7-361-2014, 2014.

Wang, K., and Dickinson, R. E.: Global atmospheric downward longwave radiation at the surface from ground-based observations, satellite retrievals, and reanalyses, Reviews of Geophysics, 51, 150-185, 10.1002/rog.20009, 2013.

https://doi.org/10.5194/acp-2022-275
Preprint. Discussion started: 26 April 2022

Atmospheric Chemistry and Physics Discussions

Wesely, M.: Parameterization of surface resistances to gaseous dry deposition in regional-scale numerical-models, Atmos. Environ., 23, 1293–1304, https://doi.org/10.1016/j.atmosenv.2007.10.058, 1989.

Woodhouse, M. T., Luhar, A. K., Stevens, L., Galbally, I., Thatcher, M., Uhe, P., Wolff, H., Noonan, J., and Molloy, S.: Australian reactive-gas emissions in a global chemistry-climate model and initial results, Air Quality and Climate Change, 49, 31-38, 2015.

Zhong, W. and Haigh, J. D.: An efficient and accurate correlated-k parameterization of infrared radiative transfer for troposphere–stratosphere–mesosphere GCMs, Atmos. Sci. Lett., 1, 125–135, https://doi.org/10.1006/asle.2000.0022, 2000.

Zhong, W., Osprey, S. M., Gray, L. J., and Haigh, J. D.: Influence of the prescribed solar spectrum on calculations of atmospheric temperature, Geophys. Res. Lett., 35, L22813, https://doi.org/10.1029/2008GL035993, 2008.